Realizing Dynamic and Efficient Bipedal Locomotion on the Humanoid Robot DURUS

Jacob Reher[1], Eric A. Cousineau[2], Ayonga Hereid[1], Christian M. Hubicki[1], and Aaron D. Ames[3]

***Abstract*— This paper presents the methodology used to achieve efficient and dynamic walking behaviors on the prototype humanoid robotics platform, DURUS. As a means of providing a hardware platform capable of these behaviors, the design of DURUS combines highly efficient electromechanical components with "control in the loop" design of the leg morphology. Utilizing the final design of DURUS, a formal framework for the generation of dynamic walking gaits that maximizes efficiency by exploiting the full body dynamics of the robot, including the interplay between the passive and active elements, is developed. The gaits generated through this methodology form the basis of the control implementation experimentally realized on DURUS; in particular, the trajectories generated through the formal framework yield a feed-forward control input which is modulated by feedback in the form of regulators that compensate for discrepancies between the model and physical system. The end result of the unified approach to control-informed mechanical design, formal gait design and regulator-based feedback control implementation is efficient and dynamic locomotion on the humanoid robot DURUS. In particular, DURUS was able to demonstrate dynamic locomotion at the DRC Finals Endurance Test, walking for just under five hours in a single day, traveling 3.9 km with a mean cost of transport of 1.61—the lowest reported cost of transport achieved on a bipedal humanoid robot.**

I. INTRODUCTION

The humanoid robot, DURUS, was revealed to the public at the DARPA Robotics Challenge (DRC) Robot Endurance Test in June 2015 [1]. Developed by SRI International, DURUS was designed with the overarching goal of achieving never before seen efficiency in locomotion, thereby allowing for longer autonomous battery-powered operation. This goal is in response to the current state of the art in humanoid robots. While there have been dramatic increases in capabilities for performing tasks and navigating terrain through semi-autonomous task-based operation—as seen in the DRC Finals—this is often achieved at the cost of increased energy usage. The results presented in this paper take the opposite perspective by prioritizing a single objective: achieve maximum efficiently in locomotion through a holistic design, control and implementation methodology, with a focus on utilizing the full body dynamics of the robot—leveraging passive mechanical elements—to realize dynamic walking.

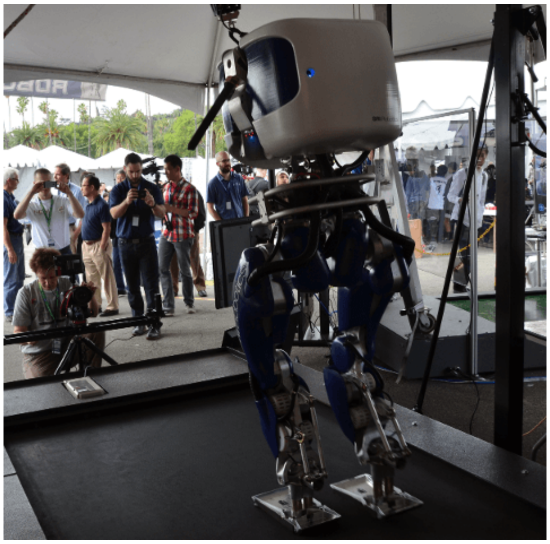

Fig. 1: Humanoid robot DURUS exhibiting dynamic walking behaviors at the DARPA Robotics Challenge Endurance Test.

Traditional approaches for locomotion prioritize the ability to complete a wide-variety of tasks, e.g., step placement, turning, and stair climbing, over achieving highly dynamic and efficient locomotion. At the core of most methods employed on robots today is a low-dimensional representation of the full-order robot which utilizes a heuristic notion of stability known as the Zero Moment Point (ZMP) criterion [16], [25], and an extension termed Capture Point [20]. The ZMP and capture point methods are robust and allow for a variety of walking behaviors; however, the resulting locomotion is typically slow and very energy consuming. More recently, there have been several optimization based controllers [10], [17], [8], [9], [24] proposed in response to the DARPA Robotics Challenge. However, these approaches have been applied mainly with ZMP and capture point heuristics coupled with constraints, offer no formal guarantees, and again lack efficiency. With a view towards creating highly efficient walking, the passive dynamics community [18], [6], [4], [28] has aimed to utilize the passive dynamics of the robot to attain efficient walking with minimal power injection from actuators. While these walkers can achieve very efficient walking, e.g., the Cornell Ranger has the lowest recorded cost of transport for a legged robot of 0.19 [5], the design typically involves the use of many passive elements such as free-swinging joints and small actuators which make implementation difficult on a robot which must also have the ability to locomote and still perform a variety tasks.

This work is supported by the DARPA M3A Program and NSF grants CPS-1239055, NRI-1526519

[1] Jacob Reher, Ayonga Hereid, and Christian M. Hubicki are with the Woodruff School of Mechanical Engineering, Georgia Institute of Technology, Atlanta, GA, 30332 USA

[2] Eric Cousineau is with Mathworks Inc. and is a previous member of the AMBER Lab

[3] Aaron D. Ames is with the Woodruff School of Mechanical Engineering and the School of Electrical and Computer Engineering, Georgia Institute of Technology, Atlanta, GA, 30332, USA

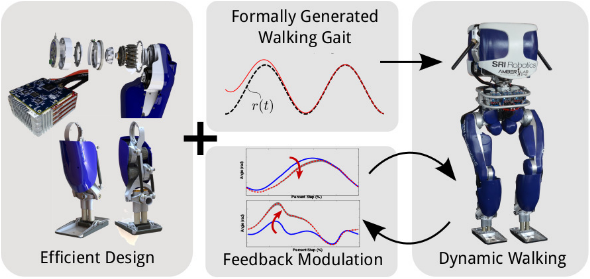

Fig. 2: Approach to implementing efficient locomotion on DURUS. Specificially, a formally stable walking gait is used for time-based position tracking on hardware. A regulator structure then perturbs the trajectories on the torso roll, hip roll, and hip yaw joints for stabilization.

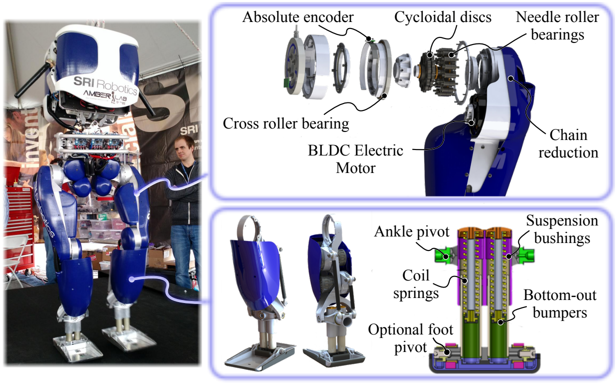

Fig. 3: Novel mechanical components used on DURUS in order to improve efficiency in locomotion.

This paper presents the methods used to demonstrate dynamic and efficient walking on the humanoid robot, DURUS, experimentally. This methodology begins with the design of dynamic and efficient walking gaits on bipedal robots through hybrid zero dynamics (HZD) [2], [12], [15], [26], [27], a mathematical framework that utilizes hybrid systems models coupled with nonlinear controllers that provably results in stable locomotion. In particular, we utilize HZD to formulate a nonlinear optimization problem for DURUS that accounts for the full-body dynamics of the robot in order to maximize the efficiency of the gait. The end result is a nonlinear controller that provably produces stable robotic walking [2]. The resulting trajectories are realized on the hardware via a feedforward term that encodes the formal gait design. To account for differences between the physical robot and the ideal model, a heuristic feedback is added to the control implementation in the form of regulators that modulate joints based upon environmental perturbations. The control framework presented allows for the full utilization of novel mechanical components on DURUS, including: efficient cycloidal gearboxes which allow for almost lossless transmission of power and compliant elements at the ankles for absorbing the impacts at foot-strike.

At the core of the control architecture implemented on DURUS is the underlying assumption that the dynamics of the electromechanical system will operate near those of the desired system. The low-level motor controllers of the robot ensure that the formally generated trajectories will be closely tracked, with 0.005 rad rms tracking error for the experiments documented in this paper. Also, due to the relatively small stabilizing perturbations induced by the feedback regulators, the walking trajectories demonstrated on DURUS in this work are shown to preserve 83.3% of the “formal” gait. Additionally, through the combination of formal controller design and novel mechanical design, the humanoid robot DURUS was able to achieve a mean electrical cost of transport of 1.61 over roughly five hours of continuous walking—the lowest recorded electrical cost of transport for a bipedal humanoid robot.

The presented work is structured as follows: The overview of the mechanical components, which provide an efficient basis for which the control strategy builds upon, is described in Sec. II. The mathematical modeling of DURUS is presented in Sec. III. The control approach, including the formal feedforward gait construction and the feedback regulator structure are detailed in Sec. IV. Finally, the experimental results are presented in Sec. V.

II. DESIGN

The underlying mechanical and electrical components incorporated into the design of DURUS provide an essential foundation from which the control design can build upon. In particular, a two-pronged approach was taken in the design of DURUS: (1) novel mechanical and electrical components providing significant gains in efficiency and (2) a leg morphology which was the result of an iterative feedback loop between mechanical design and control synthesis. The components resulting from this approach are shown in Fig. 3.

Novel Components. The primary mechanical components which provided gains in overall efficiency were the actuator and transmission elements (see Fig. 3). Each actuator-gearbox combination consisted of an electric motor connected via a chain reduction to a custom-designed cycloid transmission, which can achieve up to 97% efficiency. Each actuator-gearbox unit was lightweight, weighing only 2.7 kg and able to output 250 Nm of torque with maximum joint accelerations exceeding 130 rad/s^2.

To ultimately realize dynamic and efficient locomotion on the humanoid robot DURUS, precision in control implementation is required at every level of the hardware. Therefore, an essential component in the process of realizing locomotion is a motor controller which can accurately track the trajectories generated in Sec. IV accurately. Custom motor controllers are employed on DURUS, allowing for 10 kHz control of torque, current, and position. For the duration of the walking analyzed in Sec. V, these motor controllers tracked joint positions with an overall *rms* error of 0.005 rad and a peak error of 0.026 rad. Additionally, DURUS is self-powered with a 1.1 kWh battery pack weighing 9.5 kg.

Control in the Loop Design. The morphology of DURUS, and specifically the role of passive-compliant elements, di-

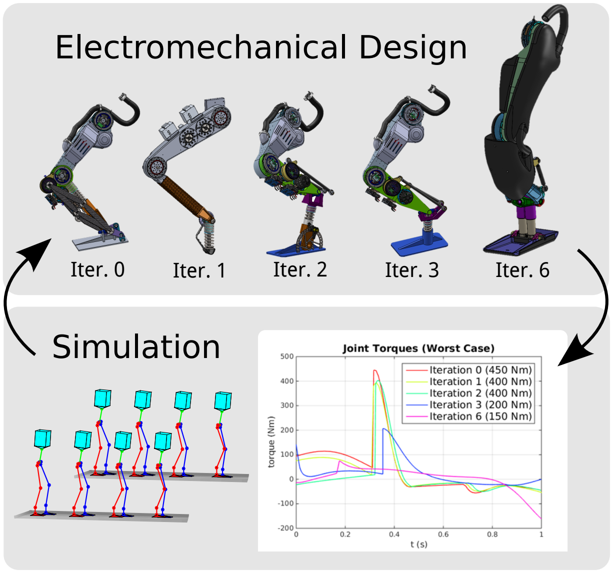

Fig. 4: Iterative design process which facilitated a leg morphology satisfying hardware constraints in simulation.

rectly impacted how well a control scheme could achieve efficient and stable dynamic gaits both in simulation and experimentally. The leg morphology of DURUS is the result of an iterative collaboration between the designer and control engineers. Specifically, designs for the leg geometry and passive-compliant ankles were passed to rigorous simulation for evaluation. In particular, the nonlinear control and gait approach in [14] was utilized to realize walking in simulation and the design was evaluated with regard to performance parameters such as the joint torques and walking stability. These findings were then compiled and passed back to the design engineer for improvement. The result of this iterative process was a leg design which walked in simulation with worst case torques of 150 Nm, as opposed to initial leg designs which demonstrated peak torques of 450 Nm; this procedure, along with several of the leg designs and their associated simulation torques, is illustrated in Fig. 4. The authors believe that this "control in the loop" mechanical design methodology was a key factor in the ability of the control scheme presented in Sec. IV to maintain smooth, stable walking while exploiting the energy saving capabilities of the passive-compliant ankle structures.

A key difference between DURUS and many humanoid robots is the use of passive springs in the ankles with significant compliance. To leverage the greatest returns, the springs are much more compliant than typically seen on powered humanoid robots leveraging springs for efficiency [21], [30]. This level of compliance in DURUS allows for the design of gaits which can be designed with significant energy savings at impact. The drawback to this compliance is the injection of additional passive degrees of freedom in the robot which are difficult to control. This difficulty motivates a nonlinear control method and gait design procedure which formally guarantees stable walking on the model of the robot.

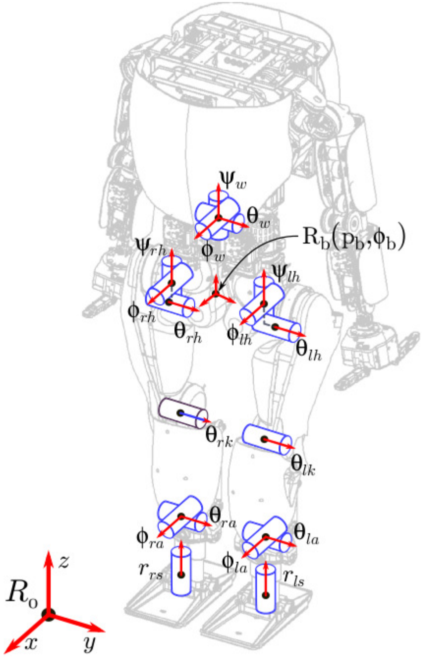

Fig. 5: The coordinate system used on DURUS.

III. Robot Model

The underlying model of DURUS differs from many humanoid robots currently in use due to the passive springs in the feet. These passive elements are included in the model and control design so that gaits that exploit them can be generated in order to realize efficient walking. However, the high degree of compliance in the ankles introduces nontrivial complexity to the dynamics of the robot. As such, it is crucial that a model is constructed of the robot which can formally represent the distinct modes of the walking gait. This work uses a two domain hybrid model [14] consisting of a *double-support*, $\mathscr{D}_{\rm ds}$, and a *single-support* domain, $\mathscr{D}_{\rm ss}$. In this section, the overall configuration, hybrid model, and dynamics used in Sec. IV are laid out for DURUS.

Robot Configuration. The configuration of the robot body, as illustrated in Fig. 5, consists of three kinematic chains: waist joints, $q_w = [\psi_w, \varphi_w, \theta_w]^T$, left leg joints, $q_l = [\psi_{lh}, \varphi_{lh}, \theta_{lh}, \theta_{lk}, \theta_{la}, \varphi_{la}, r_{ls}]^T$, and right leg joints, $q_r = [\psi_{rh}, \varphi_{rh}, \theta_{rh}, \theta_{rk}, \theta_{ra}, \varphi_{ra}, r_{rs}]^T$, respectively, where ψ_w, φ_w, and θ_w are the waist yaw, roll, and pitch angles, ψ_{lh}, φ_{lh}, θ_{lh}, θ_{lk}, θ_{la}, φ_{la}, and r_{ls} are the left hip yaw, left hip roll, left hip pitch, left knee pitch, left ankle pitch, left ankle roll angle, and left spring deflection, respectively, and ψ_{rh}, φ_{rh}, θ_{rh}, θ_{rk}, θ_{ra}, φ_{ra}, and r_{rs} are the right hip yaw, right hip roll, right hip pitch, right knee pitch, right ankle pitch, right ankle roll angle, and right spring deflection, respectively. To compose the floating base coordinates for the robot, a fixed world frame R_0 is considered along with a body reference frame R_b attached to the pelvis.

The generalized configuration space of the robot is described by the generalized coordinates $q = (p_b, \varphi_b, q_r) \in \mathscr{Q} \subset \mathbb{R}^n$ where there are $n = 23$ coordinates and $\mathscr{Q}$ is the configuration space of the robot (viewed as a subset of $\mathbb{R}^n$).

Hybrid Model. Having introduced the joint configuration of DURUS, the two-domain hybrid system model for DURUS can be defined based on the framework established in [23], [15]. In particular, we specify the robotic system as the tuple:

$$\mathscr{HC} = (\Gamma, \mathscr{D}, \mathscr{U}, S, \Delta, FG), \tag{1}$$

where Γ is is a *directed cycle* specific to this walking model with verices V and edges E, $\mathscr{D} = \{\mathscr{D}_v\}_{v \in V}$ is a set of admissible domains, $\mathscr{U} = \{\mathscr{U}_v\}_{v \in V}$ is a set of admissible controls, $S = \{S_e \subset \mathscr{D}_v\}_{e \in E}$ is a set of *guards* or *switching surfaces*, $\Delta = \{\Delta_e\}_{e \in E}$ is a set of *reset maps*, and $FG = \{FG_v\}_{v \in V}$ is a set of affine control systems defined on $\mathscr{D}_v$.

The two domains of the robot upon which the hybrid system is modeled depends on the current status of the foot contact points with the ground. The robot is in the double-support (DS) domain when both feet are in contact with the ground and transitions to single-support (SS) domain when one of the legs lifts off the ground. The transition from single-support to double support domain occurs when the non-stance foot strikes the ground.

The continuous dynamics of the system depends on the Lagrangian of the robot model and the holonomic constraints, such as foot contacts with the ground, defined on a given domain. With the mass, inertia and length properties of each link of the robot, the equation of motion (EOM) for a given domain $\mathscr{D}_v$ is determined by the classical Euler-Lagrange equation [19], [12]:

$$D(q)\ddot{q} + H(q,\dot{q}) = B_v u_v + J_v^T(q) F_v, \tag{2}$$

where $v \in \{\mathrm{ds}, \mathrm{ss}\}$, $D(q)$ is the inertia matrix including the reflected motor inertia, $H(q,\dot{q}) = C(q,\dot{q})\dot{q} + G(q) + \kappa(q,\dot{q})$ is a vector containing the Coriolis term, the gravity vector, and the spring force vector, B_v is the distribution matrix of actuators, and F_v is a collection of contact *wrenches* containing the external forces and/or moments exerting on the robot due to the holonomic constraints (see [19]). The Jacobian of the holonomic constraints, $J_v(q)$, is determined through the enforcement that the contact wrenches satisfy the second order differentiation of each constraint is zero. Finally, the solution for the contact wrenches is substituted into $J_v(q)$ and combined with (2) to obtain the affine control system [23], $\dot{x} = f_v(q,\dot{q}) + g_v(q)u_v$, where $x = (q,\dot{q}) \in \mathbb{R}^{2n}$ are the states of the system.

IV. Control Design

To compliment the efficient design of the robot, a control approach which leverages the passive dynamics of the robot while providing stability through the dynamic walking motions is introduced. First, a formal mathematical framework that utilizes hybrid systems models coupled with nonlinear controllers and an optimization that provably results in the generation of stable walking trajectories is introduced. Implementation of these trajectories on hardware is realized through their time-based playback on embedded level position controllers, which we term the *feedforward* component of the control implementation. Finally, a heuristic feedback control structure is added to regulate and stabilize the robot about the formal walking trajectories and again implemented at the embedded level; this is referred to as the *feedback* control component. Specifically, joints are controlled at the embedded level through desired trajectories of the form:

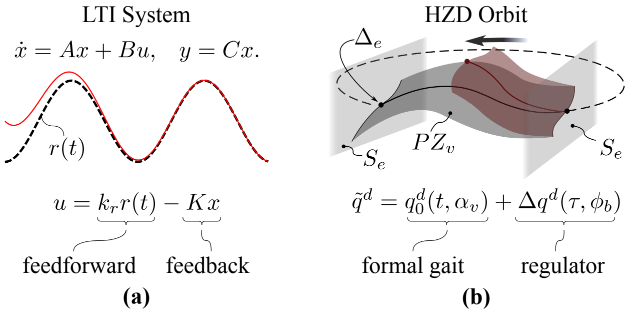

LTI System
$\dot{x} = Ax + Bu, \quad y = Cx.$
$r(t)$
$u = \underbrace{k_r r(t)} - \underbrace{Kx}$
feedforward
feedback
(a)
HZD Orbit
Δ_e
PZ_v
S_e
S_e
$\tilde{q}^d = \underbrace{q_0^d(t,\alpha_v)} + \underbrace{\Delta q^d(\tau,\phi_b)}$
formal gait
regulator
(b)

Fig. 6: The control approach implemented on DURUS (a) can be summarized as the combination of a formally generated feedforward term and stabilizing feedback term. The stabilizing feedback control perturbs the trajectories in an attempt to drive the system back onto the HZD surface (b).

$$\tilde{q}^d = \underbrace{q_0^d(t,\alpha_v)}_{\text{feedforward}} + \underbrace{\Delta q^d(\tau,\varphi_b)}_{\text{feedback}} \tag{3}$$

where q_0^d is the feedforward trajectory, α_v are the parameters of the vurtual constraints determining the HZD and found through optimization, τ is a state based parameterization of time, φ_b is the orientation of the body reference frame, and $\Delta q^d(\tau,\varphi_b)$ is the perturbation induced by the regulators.

A. Feedforward Control

A feedforward control scheme which generates a stable walking gait leveraging the passive-compliant elements in the system is presented in this section. The walking gait is the result of a nonlinear optimization problem and ultimately generates the time-based trajectories which compose the feedforward component of the control implementation.

Virtual Constraints. Analogous to holonomic constraints, virtual constraints are defined as a set of functions that regulate the motion of the robot with a certain desired behavior [2], [31], with the key difference that the holonomic constraints are realized through control inputs, rather than contact wrenches. We start by defining the outputs on the robot that will be used in the next section to modulate the walking behavior. Inspired by [3], the linearized forward hip velocity, $y_{1,v}^a(q,\dot{q}) = \delta\dot{p}_{hip}(q,\dot{q})$, is picked as the velocity-modulating output for both domains, where $\delta p_{hip}(q)$ is the linearized hip position of the robot.

Position-modulating outputs are chosen for each domain [2]. The number of outputs chosen per domain is determined by the number of available degrees of freedom in the respective domain. The double support domain, $\mathscr{D}_{\mathrm{ds}}$, is described by the nine outputs: stance knee pitch, stance torso pitch, stance ankle roll, stance torso roll, stance hip yaw, waist roll, waist pitch, waist yaw, and non-stance knee pitch. In single support, $\mathscr{D}_{\text{ss}}$, the non-stance foot is no longer constrained to the ground so five additional outputs are introduced: the non-stance slope, non-stance leg roll, non-stance foot roll, non-stance foot pitch, and non-stance foot yaw.

With the definition of the outputs in hand, virtual constraints are defined as the difference between the actual and desired outputs of the robot [2], [26], [31]:

$$y_{1,v}(q,\dot{q},v_d) = \dot{y}^a_{1,v}(q,\dot{q}) - v_d, \tag{4}$$

$$y_{2,v}(q,\alpha_v) = y^a_{2,v}(q) - y^d_{2,v}(t,\alpha_v), \tag{5}$$

for $v \in V$, where $y_{1,v}$ and $y_{2,v}$ are relative degree 1 and (vector) relative degree 2 by definition, respectively. Moreover, a forth-order Bézier polynomial is adopted to specify each desired output as in [27].

Gait Generation. With the goal of driving the outputs to zero exponentially, we consider the feedback linearizing controller formulated in [2]. The application of this control method yields linear outputs of the form:

$$\dot{y}_{1,v} = -\varepsilon y_{1,v}, \tag{6}$$

$$\ddot{y}_{2,v} = -2\varepsilon \dot{y}_{2,v} - \varepsilon^2 y_{2,v}, \tag{7}$$

for $v \in V$ with V the set of vertices for Γ given in (1)

When the control objective is met such that $y_{2,v} = 0$ for all time then the system is said to be on the partial zero dynamics surface [2]:

$$\mathbf{PZ}_{\alpha,v} = \{x \in \mathbb{R}^{2n} : y_{2,v}(x,\alpha_v) = 0, L_f y_{2,v}(x,\alpha_v) = 0\}. \tag{8}$$

This surface will be rendered invariant through the use of the control law over the continuous dynamics of the system. However, it is not necessarily invariant through the discrete impacts which occur when the swing foot comes in contact with the switching surface. As a result, the parameters α_v of the outputs must be chosen in a way which renders $\mathbf{PZ}_{\alpha,v}$ invariant through impact, i.e., which yield partial hybrid zero dynamics (PHZD) and can be formulated as a constrained nonlinear optimization problem [2]:

$$\alpha_v^* = \underset{\alpha_v}{\text{argmin}}\ \text{Cost}(\alpha_v) \tag{9}$$

$$\text{s.t} \quad \Delta_e(S_e \cap \mathbf{PZ}_{\alpha,v}) \subseteq \mathbf{PZ}_{\alpha,v}, \tag{PHZD}$$

for all $e \in E$, where the cost is the mechanical cost of transport for the walking gait. This optimization problem is then reformulated in the context of a direct collocation method, given in [13].

To effectively implement the walking gait produced from the optimization problem on hardware, the desired joint and angular velocities of the robot in each iteration must be found. To obtain a set of time-based trajectories for playback on the physical hardware, DURUS is simulated using the feedback linearizing controller in [2] and the parameter set obtained from the optimization. The joint trajectories of the stable walking in simulation are recorded and stored as a set of time-based positions and velocities for tracking:

$$q_0^d(t,\alpha_v) = q^a_{sim}(c_{\text{ff}}t,\alpha_v) \tag{10}$$

$$\dot{q}^d(t,\alpha_v) = \dot{q}^a_{sim}(c_{\text{ff}}t,\alpha_v) \tag{11}$$

where c_{ff} is a scaling constant which is used to allow for the walking trajectories to be sped up or slowed down when implemented on hardware as the feedforward term in (3).

B. Feedback Control.

While the feedforward time-based trajectories, q_0^d, are generated with the dynamics of the system in mind, it quickly became evident as gaits were implemented on DURUS that regulating feedback control would be crucial to stabilize the system for long-duration walking. The authors adopted a regulator design similar to those of [11], [22], but with a focus on position control. In particular, taking the actual and desired objectives for a given regulator, a trajectory perturbation was heuristically calculated and incorporated into the formally generated trajectories to yield a system which was responsive to minor destabilizations such as unmeasured compliance or environmental factors. The primary function of these trajectory perturbations is to smoothly stabilize the robot in the lateral (roll) direction and to steer the robot.

The feedback component of the controller is achieved through two regulators: a roll regulator for lateral stability and a yaw regulator for walking direction control. These regulators were implemented using discrete logic to handle a smooth blending factor dependent on the current discrete domain ($\mathscr{D}_{\text{ds}}$ or $\mathscr{D}_{\text{ss}}$) and therefore prevents large jumps in the commanded position that can occur through the transitions between domains. The discrete logic of the blending factor is implemented using the global phase variable, τ, which is the normalization of the position of the hip from the beginning to end of the step. Through the course of each step, a normalized phase variable, λ, is calculated as:

$$\lambda = \frac{\tau - \tau_{min}}{\tau_{max} - \tau_{min}}, \tag{12}$$

where τ_{max} and τ_{min} are the maximum and minimum values of τ as generated in the formal walking gait.

The implementation of the blending factor (s), and how it behaved with regard to the spring based switching, played a critical role in the behavior that the regulators induced. Throughout the single-support domain, $\mathscr{D}_{\text{ss}}$, the non-stance leg blending factor s_{ns} was increased according to λ, starting from a magnitude of zero and finishing at one as the swing phase ends. The stance leg blending factor s_s is decreased at a rate faster than the duration of the whole domain using an acceleration factor c_{fb}. The single-support blending factor update can be summarized as:

$$s_{ns} = \lambda, \qquad s_s = -c_{\text{fb}}\lambda, \tag{13}$$

where $s \leftarrow s + \Delta s$ in each cycle. During the double-support domain, $\mathscr{D}_{\text{ds}}$, the blending factor is held constant, such that each of the legs do not oppose the motion of the other. This blending factor feature will be used in the following sections to regulate the allowable trajectory perturbations in each of the discrete-mode feedback controllers.

Roll Regulator. The main stabilizing action of the roll regulator is to abduct the hip joint of the swing leg throughout the single support phase. This hip abduction effectively changes the location of the foot strike, placing it in a more desirable configuration for recovering from a lateral sway. Also incorporated into the roll regulator is a waist roll action which moves the torso away from a position in which it might topple over the stance leg after impact. The feedback controller then takes on the form of a proportional controller:

$$\Delta q^d = -s_i k \left(y^a - y^d\right), \qquad i \in \{s, ns\}, \tag{14}$$

where $y^a := \varphi^{\text{imu}}_{torso,roll}$ and $y^d := \varphi^{\text{computed}}_{torso,roll}$ are the actual torso orientation from the IMU and the torso orientation computed via the robot kinematics assuming a flat foot in contact with the ground.

Yaw Regulator. The yaw regulator uses user input via a joystick controller as the desired objective. While operating the robot on a treadmill, the electromagnetic interference was sufficient to render the heading information from the magnetometer unusable thus the actual heading is set to zero. This allows the user to modulate the steering action about the current direction that DURUS is facing. The desired effect of this regulator is to yaw the hip joint while the leg is in swing during single-support in order to change the orientation with which the foot will strike the ground. After double support, the hip yaw is blended away with the foot planted, turning DURUS about the stance leg and into the desired direction. The regulator is of the same proportional form as (14) where $y^a := 0$ and $y^d :=$ joystick input (see Fig. 7).

C. *Control Implementation.*

The control software infrastructure followed that of [7]. Specifically, each joint on the robot had a corresponding microcontroller communicating with a real-time (RT) process. This RT process relays data to and from a lower priority real-time process implemented in C++ to perform high-level control. The high-level control is relatively simple: the hardware coordinates are transformed into model coordinates via a transmission, then the pre-recorded trajectories played back with the regulators superimposed to yield the desired profiles of each joint as in (3). Finally, the model coordinates are transformed back into hardware coordinates.

From the high-level, desired joint trajectories travel through two stages before reaching the low-level embedded control. First, desired motor positions are sent from the high-level process to the Simulink-generated process responsible for communicating with the joint microcontrollers. At this stage, the trajectory is up-sampled from 250 Hz to 1 kHz with a first-order hold and sent to the embedded level. An IMU mounted in the torso of DURUS is used to determine the global orientation of the torso for the roll regulator. Finally, incremental encoders and absolute encoders are used at each joint, though incremental encoders are the only sensors used actively in the joint-level feedback control. The joint microcontrollers implement the modulated joint trajectories (3) and the joint velocities from (11) via position control at 10 kHz. The discrete modes of the regulator structure are triggered by the foot interactions with the ground; specifically, strike detection is triggered when the spring deflection in the ankles passes a certain threshold. The results of applying the regulators to DURUS while walking, including the discrete structure of the blending factor together with actual and desired values in (14) and the resulting applied delta, Δq^d, is shown in Fig. 7.

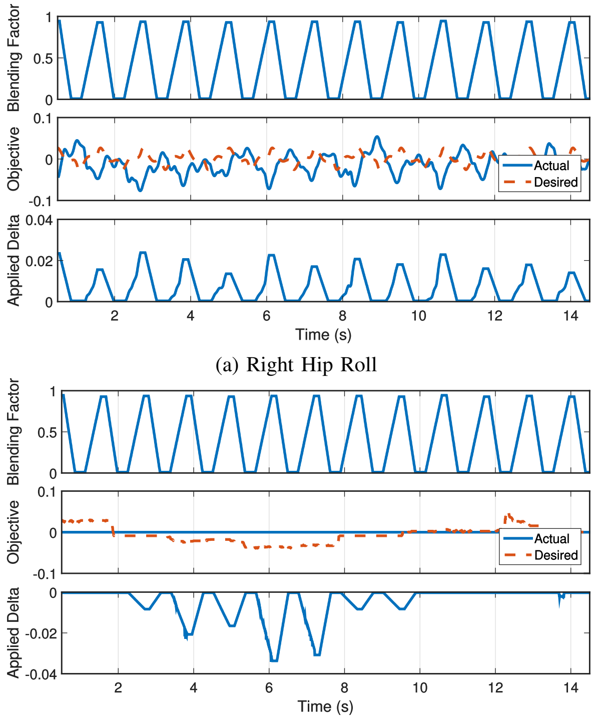

(a) Right Hip Roll

(b) Right Hip Yaw

Fig. 7: Regulator variables for right hip yaw and roll joints. The dashed objective is directly controlled from a joystick to steer the robot in the yaw regulator and is the desired torso roll in the roll regulator. Pictured are several steps during which a user steered the robot with a left-right-left action.

V. RESULTS

The Robot Endurance Test at the DRC Finals took place over two days, during which DURUS exhibited sustained walking over large distances with a consistently low cost of transport [1]. These results were realized through the application of the formal techniques previously discussed coupled with a stabilizing regulator structure. The longest of these walking runs took place during the second day, during which DURUS walked on two consecutive batteries and exceeded walking distances of 3.8 km. A summary of the walking for this day is summarized in Table I.

Walking data was periodically recorded in ten minute segments while demonstrating the robot to the public. Live

TABLE I: Walking Statistics

Battery	Duration (hh:mm:ss)	Distance Traveled (meters)	$\bar{c}_{et}$ (mean)
1	2:35:43	2055.0	1.57
2	2:17:12	1812.8	1.69
TOTAL	4:52:55	3867.8	1.61

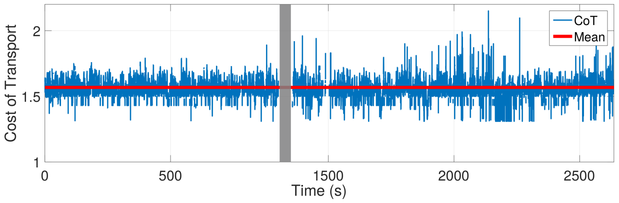

Fig. 8: Available data for cost of transport on the first battery charge as measured at the DARPA Robotics Challenge Robot Endurance Test. Grey area indicates time during which data was not being recorded.

performance metrics, including the electrical cost of transport, were available on a screen displayed next to DURUS. The cost of transport data available for the duration of the experimental run on one battery charge is plotted in Fig. 8. The specific cost of electrical transport c_{et} is calculated as in [7], where the total energy consumed over the weight and distance traveled is represented for step i as:

$$c_{et,i} = \frac{1}{mgd_i} \int_{t_i^+}^{t_i^-} P_{el}, \tag{15}$$

where P_{el} is the consumed power and d_i is the x-position traveled by the non-stance foot of the robot through the duration of the i^{th} step. Power data was computed directly from current and voltage measured on the battery pack which supplies power to all components on the robot.

In this work, energy efficiency is used as a metric in which to evaluate the mechanical design and control implementation. The reported electrical cost of transport for several robots is summarized in Table II, from which we observe the robots utilizing passive elements, small motors, or anthropomorphic designs to leverage energy savings demonstrating the lowest energy expenses (Cornell Ranger and Biped). Additionally, robots employing HZD to achieve locomotion exhibit efficient locomotion (AMBER 1 and 2D-DURUS), although these are restricted to walking in a 2D plane. The closest efficiency numbers come from ATRIAS—possibly since it inspired the compliment elements in the design of DURUS—yet this robot is not humanoid in nature. Therefore, in the category of full-scale bipedal humanoid robots (e.g., ATLAS and ASIMO) the electrical cost of transport on DURUS is the lowest ever reported.

TABLE II: Comparison of Efficiency on Various Platforms

Name	$\bar{c}_{et}$	m (kg)
Human	0.2	·
ATLAS [5]	5	102
ASIMO [6]	3.23	52
AMBER 1 [29]	1.88	3.3
ATRIAS [22]	1.13	62
2D-DURUS [7]	0.63	31.5
Cornell Biped [6]	0.2	13
Cornell Ranger [5]	0.19	9.9
DURUS	1.61	79.5

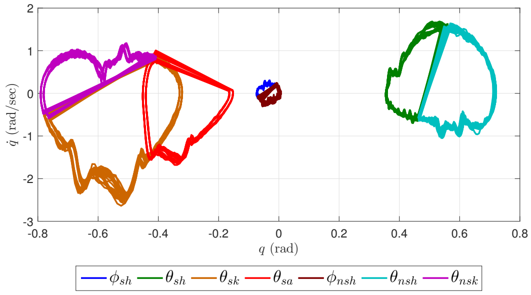

Fig. 9: In the context of bipedal walking, a stable limit cycle implies stable walking. These limit cycles exhibit a closed behavior, indicating that they represent stable walking on DURUS for both the saggital and coronal planes.

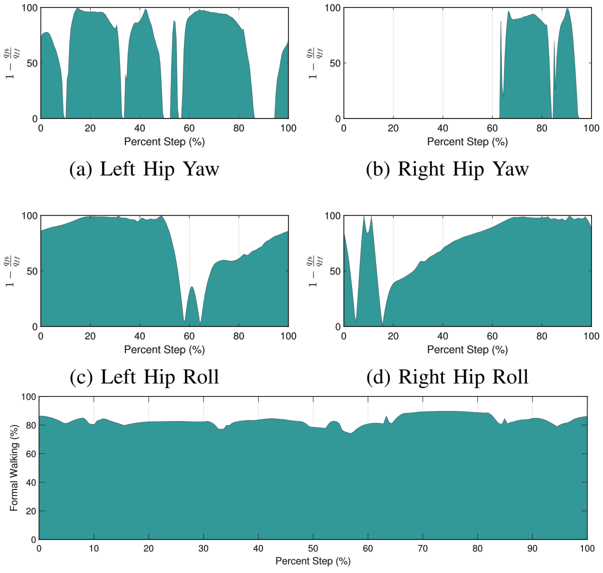

(a) Left Hip Yaw

(b) Right Hip Yaw

(c) Left Hip Roll

(d) Right Hip Roll

(e) Percent Formal Walking

Fig. 10: Percent of formal walking trajectories preserved on DURUS. Pictured is the mean formal effort over the course of a step interval for 10 minutes of walking data.

A core contribution of this paper is the use of formal nonlinear control methods to realize dynamic walking on humanoid robots. To quantify the degree to which the formal walking behavior is realized, we quantify the percentage of formal walking present in the gait experimentally through:

$$\%q^f = \frac{1}{n} \sum_{j=1}^{n} 1 - \frac{\Delta q_j^d(\tau,\theta)}{q_{0,j}^d(t,\alpha)}, \tag{16}$$

for the $n = 17$ joints. The mean of 1588 steps over a 10 minute interval is shown in Fig. 10. Pictured are means of several of the regulated joints along with the mean percent formal walking of the total system. Specifically, the mean percent formal walking exhibited on DURUS was $\%\bar{q}^f = 83.3\%$. Fig. 11 shows a visual comparison of the walking gait in simulation and experimentation over one step.

VI. CONCLUSIONS

This paper presented the methodology by which efficient locomotion was achieved on the humanoid DURUS. The

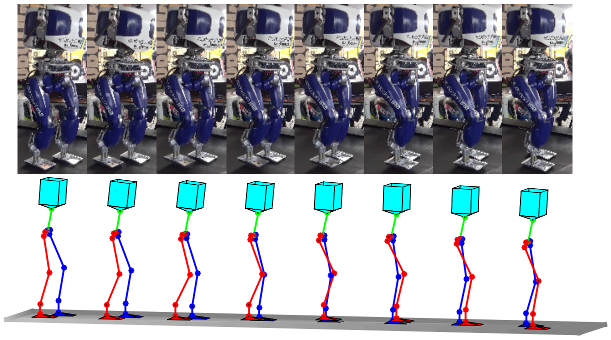

Fig. 11: Walking gait snapshot comparison of experimental and simulated results for DURUS over one step.

electromechanical design of the robot was introduced, with a special focus on components that improved efficiency along with the "control in the loop" leg design morphology that determined the configuration of passive compliant elements. The mechanical design was utilized in a the formal design of stable walking gaits which exploit the full body dynamics of the robot. To stabilize the resulting trajectories on the robot when implemented experimentally, a preliminary heuristic regulator-based feedback control strategy was presented. The resulting walking achieved on DURUS was shown to be stable and achieved consistently low electrical costs of transport while preserving a majority of the walking behaviors which give formal guarantees for the ideal system.

Acknowledgment

The authors would like to thank SRI for the design, development, and testing of DURUS, others in the AMBER Lab, Jessy Grizzle, and our collaborators in Dr. Jonathan Hurst's Dynamic Robotics Laboratory at Oregon State University.

References

[1] Dynamic walking on durus (aka proxi) at the 2015 drc finals. `https://youtu.be/a-R4H8-8074`.

[2] A. D. Ames. Human-inspired control of bipedal walking robots. *Automatic Control, IEEE Transactions on*, 59(5):1115–1130, 2014.

[3] A. D. Ames, E. A. Cousineau, and M. J. Powell. Dynamically stable robotic walking with NAO via human-inspired hybrid zero dynamics. In *Hybrid Systems: Computation and Control*, Beijing, 2012.

[4] S. O. Anderson, M. Wisse, C. G. Atkeson, J. K. Hodginsand G. J. Zeglin, and B. Moyer. Powered bipeds based on passive dynamic principles. In *5th IEEE/RAS International Conference on Humanoid Robots*, pages 110–116, 2005.

[5] Pranav A Bhounsule, Jason Cortell, Anoop Grewal, Bram Hendriksen, JG Daniël Karssen, Chandana Paul, and Andy Ruina. Low-bandwidth reflex-based control for lower power walking: 65 km on a single battery charge. *The International Journal of Robotics Research*, 33(10):1305–1321, 2014.

[6] S. H. Collins, A. Ruina, R. Tedrake, and M. Wisse. Efficient bipedal robots based on passive-dynamic walkers. *Science*, (307):1082–1085, 2005.

[7] Eric Cousineau and Aaron D Ames. Realizing underactuated bipedal walking with torque controllers via the ideal model resolved motion method. In *IEEE International Conference on Robotics and Automation (ICRA)*, 2015.

[8] Hongkai Dai, Andres Valenzuela, and Russ Tedrake. Whole-body motion planning with centroidal dynamics and full kinematics. In *IEEE-RAS International Conference on Humanoid Robots*, 2014.

[9] Twan Koolen *et al.* Summary of team ihmcs virtual robotics challenge entry. In *IEEE International Conference on Humanoid Robots*, 2013.

[10] Siyuan Feng, Eric Whitman, X. Xinjilefu, and Christopher G. Atkeson. Optimization-based full body control for the darpa robotics challenge. *Journal of Field Robotics*, 2015.

[11] Brent Griffin and Jessy Grizzle. Nonholonomic virtual constraints for dynamic walking.

[12] J. W. Grizzle, C. Chevallereau, R. W. Sinnet, and A. D. Ames. Models, feedback control, and open problems of 3D bipedal robotic walking. *Automatica*, 50(8):1955 – 1988, 2014.

[13] Ayonga Hereid, Eric A. Cousineau, Christian M. Hubicki, and Aaron D. Ames. 3d dynamic walking with underactuated humanoid robots: A direct collocation framework for optimizing hybrid zero dynamics. In *Robotics and Automation (ICRA), 2012 IEEE International Conference on*. IEEE, 2016.

[14] Ayonga Hereid, Christian M Hubicki, Eric A Cousineau, Jonathan W Hurst, and Aaron D Ames. Hybrid zero dynamics based multiple shooting optimization with applications to robotic walking. In *IEEE International Conference on Robotics and Automation (ICRA*, 2015.

[15] Ayonga Hereid, Shishir Kolathaya, Mikhail S Jones, Johnathan Van Why, Jonathan W Hurst, and Aaron D Ames. Dynamic multi-domain bipedal walking with atrias through slip based human-inspired control. In *Proceedings of the 17th international conference on Hybrid systems: computation and control*, pages 263–272. ACM, 2014.

[16] S. Kajita *et al.* Biped walking pattern generation by using preview control of zero-moment point. In *IEEE International Conference on Robotics and Automation*, volume 2, pages 1620–1626, 2003.

[17] Scott Kuindersma, Frank Permenter, and Russ Tedrake. An efficiently solvable quadratic program for stabilizing dynamic locomotion. In *IEEE International Conference on Robotics and Automation*, 2014.

[18] A. D. Kuo. Energetics of actively powered locomotion using the simplest walking model. *Journal of Biomechanical Engineering*, 124:113–120, 2002.

[19] Richard M Murray, Zexiang Li, and S Shankar Sastry. *A mathematical introduction to robotic manipulation*. CRC press, 1994.

[20] J. Pratt, J. Carff, S. Drakunov, and A. Goswami. Capture point: A step toward humanoid push recovery. In *IEEE-RAS International Conference on Humanoid Robots*, 2006.

[21] Jerry Pratt, *et al.* Capturability-based analysis and control of legged locomotion, part 2: Application to m2v2, a lower body humanoid.

[22] Siavash Rezazadeh, Christian Hubicki, Mikhail Jones, Andrew Peekema, Johnathan Van Why, Andy Abate, and Jonathan Hurst. Spring-mass walking with atrias in 3d: Robust gait control spanning zero to 4.3 kph on a heavily underactuated bipedal robot. *Draft*.

[23] R. Sinnet, M. Powell, R. Shah, and A. D. Ames. A human-inspired hybrid control approach to bipedal robotic walking. In *18th IFAC World Congress*, Milan, Italy, 2011.

[24] R. Tedrake *et al.* A summary of team mit's approach to the virtual robotics challenge. In *IEEE International Conference on Robotics and Automation*, 2014.

[25] M. Vukobratović, B. Borovac, and V. Potkonjak. ZMP: A review of some basic misunderstandings. *International Journal of Humanoid Robotics*, 3(2):153–175, June 2006.

[26] E. R. Westervelt, J. W. Grizzle, C. Chevallereau, J.-H. Choi, and B. Morris. *Feedback Control of Dynamic Bipedal Robot Locomotion*. Control and Automation. CRC Press, Boca Raton, FL, June 2007.

[27] E. R. Westervelt, J. W. Grizzle, and D. E. Koditschek. Hybrid zero dynamics of planar biped walkers. *IEEE Transactions on Automatic Control*, 48(1):42–56, 2003.

[28] M. Wisse and R. Q. van der Linde. *Delft Pneumatic Bipeds*, volume 34 of *Springer Tracts in Advanced Robotics*. Springer-Verlag, Berlin, Germany, 2007.

[29] S. N. Yadukumar, M. Pasupuleti, and A. D. Ames. From formal methods to algorithmic implementation of human inspired control on bipedal robots. In *Tenth International Workshop on the Algorithmic Foundations of Robotics (WAFR)*, Boston, MA, 2012.

[30] Jinichi Yamaguchi, Sadatoshi Inoue, Daisuke Nishino, and Atsuo Takanishi. Development of a bipedal humanoid robot having antagonistic driven joints and three dof trunk. In *Intelligent Robots and Systems, 1998. Proceedings., 1998 IEEE/RSJ International Conference on*, volume 1, pages 96–101. IEEE, 1998.

[31] Hui-Hua Zhao, Wen-Loong Ma, Michael B Zeagler, and Aaron D Ames. Human-inspired multi-contact locomotion with amber2. In *ICCPS'14: ACM/IEEE 5th International Conference on Cyber-Physical Systems (with CPS Week 2014)*, pages 199–210. IEEE Computer Society, 2014.